ADVANCED FUNCTIONAL MATERIALS
www.afm-journal.de

In-Plane Alignment in Organic Solar Cells to Probe the Morphological Dependence of Charge Recombination

*Omar Awartani, Michael W. Kudenov, R. Joseph Kline, and Brendan T. O'Connor**

Bulk heterojunction (BHJ) organic solar cells are fabricated with the polymer semiconductor aligned in the plane of the film to probe charge recombination losses associated with aggregates characterized by varying degrees of local order. 100% uniaxial strain is applied on ductile poly(3-hexylthiophene):phenyl-C61-butyric acid methyl ester (P3HT:PCBM) BHJ films and characterize the resulting morphology with ultraviolet-visible absorption spectroscopy and grazing incidence X-ray diffraction. It is found that the strained films result in strong alignment of the highly ordered polymer aggregates. Polymer aggregates with lower order and amorphous regions also align but with a much broader orientation distribution. The solar cells are then tested under linearly polarized light where the light is selectively absorbed by the appropriately oriented polymer, while maintaining a common local environment for the sweep out of photogenerated charge carriers. Results show that charge collection losses associated with a disordered BHJ film are circumvented, and the internal quantum efficiency is independent of P3HT local aggregate order near the heterojunction interface. Uniquely, this experimental approach allows for selective excitation of distinct morphological features of a conjugated polymer within a single BHJ film, providing insight into the morphological origin of recombination losses.

1. Introduction

In high performance organic solar cells, a bulk heterojunction (BHJ) active layer is typically employed that consists of a blend of two or more organic semiconductors, usually a conjugated polymer donor and a fullerene acceptor.[1] The performance advantage of this architecture is primarily attributed to the large increase in the dissociation of photogenerated excitons, enabled by the close proximity of the heterojunction (providing a mechanism for efficient exciton dissociation) to the location of exciton formation. Once the excitons are dissociated into free charge carriers, the BHJ morphology must also allow for efficient charge transport to the electrodes. This requires that the semiconductors that make up the BHJ are able to intermix well while maintaining a path for efficient charge collection. Thus, it is not surprising that device performance is highly sensitive to the BHJ morphology. This has lead to numerous studies that have investigated the role of BHJ morphology on various energy conversion losses.[2–11] In the majority of these studies, a variation in materials or processing methods is used to modify the BHJ morphology that is then related to a change in device performance.[3,7,8,10,12] While this approach is effective, changes in the film morphology are often coupled to a number of energy conversion processes, resulting in ambiguity associated with the change in morphology and specific loss mechanisms.

In this study, we selectively excite distinct morphological features of a conjugated polymer within a single BHJ organic photovoltaic (OPV) cell to provide insight into the spatial and morphological origin of electronic losses. This is accomplished by fabricating a BHJ film with highly aligned polymer aggregates. The focus here is on poly(3-hexylthiophene):phenyl-C61-butyric acid methyl ester (P3HT:PCBM) OPV devices, where highly aligned polymer chains have previously been fabricated using a strain alignment approach.[13] Briefly, the strain alignment process consists of physically straining a spun cast BHJ film by 100% while on an elastomer substrate, and then transfer printing the film onto a partially fabricated device. The film is thermally annealed to improve ordering, and a counter electrode is then deposited on top of the film to complete the device.[13] The large applied strain has previously been shown to effectively align P3HT aggregates with the polymer backbone aligned in the direction of strain.[13,14] Importantly, in strain aligned P3HT films, the highly ordered P3HT aggregates are strongly aligned while amorphous P3HT and lower order aggregates align to a drastically reduced extent.[14,15] As the primary optical transition dipole is parallel to the P3HT backbone,[16] illuminating with polarized light allows for preferential excitation of the aligned highly ordered aggregates or the more misaligned lower ordered aggregates, as illustrated in **Figure 1** and

O. Awartani, Prof. B. T. O'Connor
Department of Mechanical and Aerospace Engineering
North Carolina State University
Raleigh, NC 27695, USA
E-mail: brendan_oconnor@ncsu.edu
Prof. M. W. Kudenov
Department of Electrical and Computer Engineering
North Carolina State University
Raleigh, NC 27695, USA
Dr. R. J. Kline
Materials Science and Engineering Division
National Institute of Standards and Technology
Gaithersburg, MD 20899, USA

DOI: 10.1002/adfm.201403377

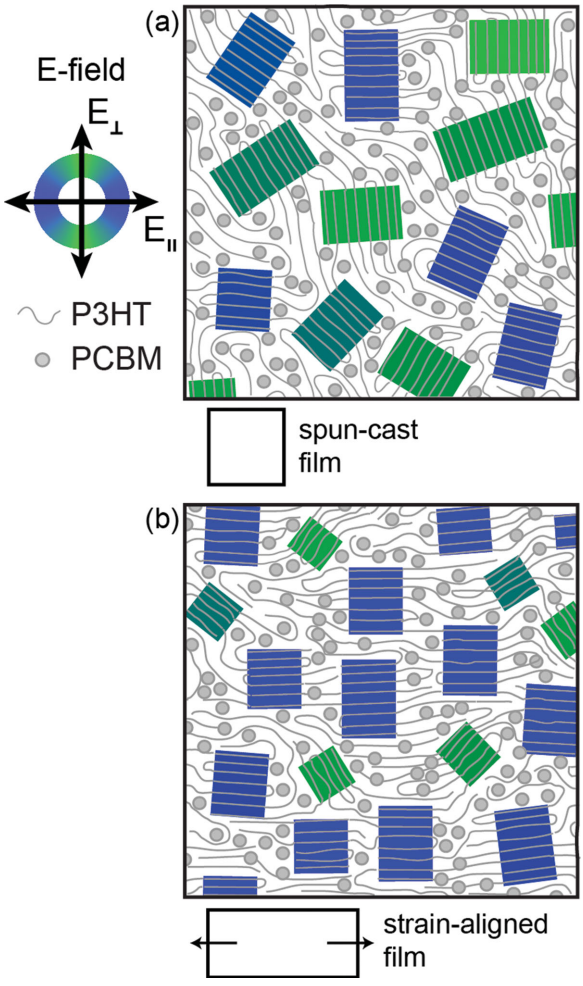

Figure 1. A simplified illustration showing the effect of strain on the morphology of the BHJ film and the absorption of the P3HT aggregates with illumination by polarized light. Left, an illustration of the E-field orientation being parallel and perpendicular to the strain direction. The color gradient represents the component of the field parallel to the P3HT aggregate backbone orientation. a) Schematic illustration of the unstrained P3HT:PCBM film with aggregates isotropically distributed in-plane. b) Illustration of strain-aligned P3HT:PCBM film with high order aggregates aligned in the direction of strain and low order aggregates with greater misalignment relative to the strain direction. Note, the colored regions represent the P3HT aggregates and the gray regions represent the amorphous P3HT and PCBM in the film.

discussed below in detail. Uniquely, the polarization sensitive BHJ film provides a framework to selectively excite morphologically distinct features of the semicrystalline polymer, while maintaining a common local environment for the sweep out of photogenerated charge carriers. In this study, we consider 4 distinct BHJ films where the main differences between films are the applied strain (0% or 100%) and film thickness. The *thick films* are approximately 220 nm thick as-cast (unstrained) and 155 nm after strain oriented. The thin films are approximately 85 nm thick as-cast and 60 nm after strained.

Performance losses in un-optimized P3HT:PCBM OPV devices have been attributed to increased charge carrier recombination due to space charge effects associated with low hole mobility.[17,18] These devices may have additional losses associated with an increased rate of bimolecular recombination independent of space charge effects.[7] The level of molecular order at the heterojunction interface may also impact the efficiency of exciton dissociation. It is currently unclear what the contribution of each loss mechanism is to the overall device performance given their common morphological dependence. Additionally, while the carriers are unable to be efficiently swept out of unoptimized devices, the spatial location of the recombination events may be distributed throughout the active layer, be located in close proximity to the location of exciton dissociation, or primarily occur near the contacts. Importantly, the aligned polymer OPV approach is able to probe photogeneration associated with disordered regions of the film while not encountering space charge related performance losses.

2. Results and Discussion

2.1. Active Layer Morphology

Critical to this study is that linearly polarized light incident in orthogonal directions excites distinct P3HT morphological features in the same OPV device. Thus, the morphology and absorption character of the films must be analyzed in detail.

To characterize light absorption in the films, we use ultraviolet-visible (UV–vis) absorption spectroscopy with polarized light. The absorbance anisotropy of the 100% strained films is provided in **Figure 2**a and Figure S1, Supporting Information. Both the thick and thin strained films show high absorbance anisotropy, reaching dichroic ratios of 7.4 and 5.3 at 605 nm, respectively. The dichroic ratio is taken as absorbance of light polarized parallel to the strain direction to absorbance of light polarized perpendicular to the strain direction. The dichroic ratios are indicative of significant alignment of the P3HT backbone in the direction of strain, consistent with strain-aligned neat P3HT films.[14] The unstrained films do not show absorbance anisotropy, indicative of no preferential in-plane alignment of P3HT chains, as expected. The absorbance also provides information about the P3HT aggregate order. The normalized absorbance of the strained films, given in Figure 2a, shows distinct absorbance features, particular at the 0–0 energy transition (at ≈605 nm) and 0–1 energy transition (at ≈550 nm). These vibronic features arise from intramolecular and intermolecular P3HT interactions and are indicative of P3HT aggregate order. This can be quantitatively described by a weakly interacting H-aggregate model previously developed by Spano.[19] The fitting parameters of the model are the exciton bandwidth (W), the 0–0 energy transition ($E_{0\text{–}0}$), and the Gaussian line width (σ). Here, W is related to the length of planar interacting chain segments, where a lower value is indicative of higher conjugation length, and σ is related to the energetic disorder, where a lower σ value indicates greater order within and between the aggregate polymer chains. The best-fit values for W and σ, for films under polarized light, are given in Figure 2b,c. $E_{0\text{–}0}$ is relatively constant for all measurements and is set to 2.0 eV. The values for σ and W vary depending on processing conditions as well as incident polarization. For unstrained films, W and σ are similar to previous reports.[18] In the strained films,

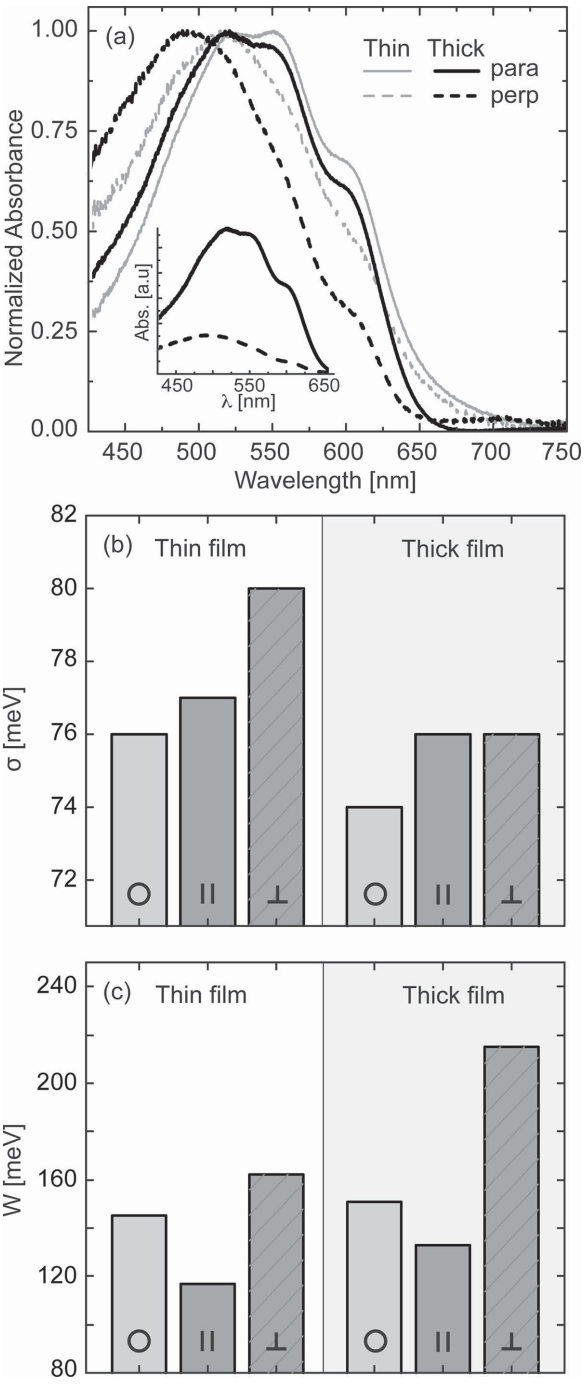

Figure 2. a) Normalized absorbance of 100% strained films under polarized light parallel (para) and perpendicular (perp) to strain direction for characteristic thick and thin films. Inset, absolute absorbance (Abs.) for the strain aligned thick film. b,c) The Gaussian line width (W) and exciton bandwidth (σ) of the absorbance measurements for the unstrained (O), and 100% strained films under polarized light parallel (||) and perpendicular (⊥) to strain direction for the thin and thick films.

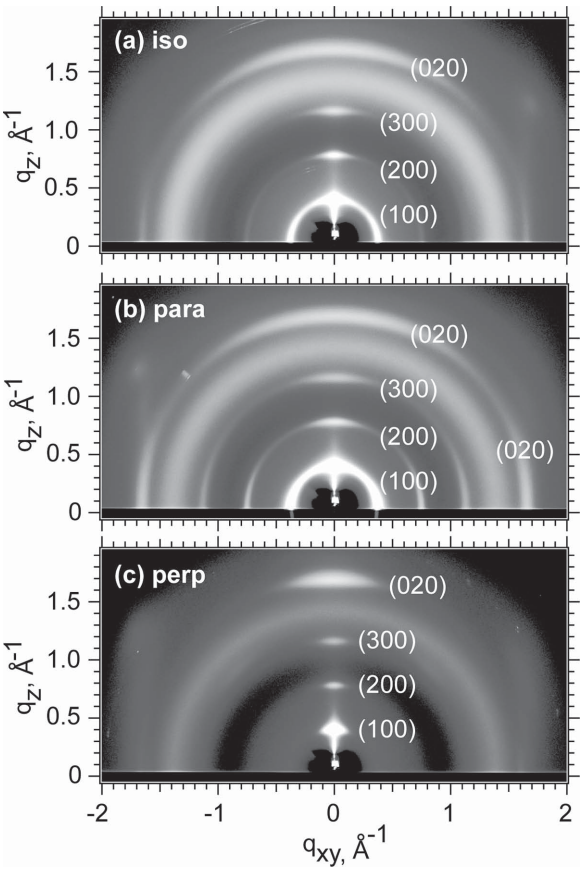

Figure 3. Grazing incidence X-ray diffraction (GIXD) image plate data for the thick a) as cast film (iso), and b,c) strain-aligned film. In the aligned film, the image plate data are for the scattering vector nominally aligned b) perpendicular (perp) and c) parallel (para) to the strain direction.

we find that σ and W have unique values depending on blend film thickness and the orientation of the incident polarized light. The key differences are that the aggregate length ($1/W$) is found to increase for aggregates that preferentially absorb parallel-polarized light, and decrease for aggregates that preferentially absorb perpendicular-polarized light, as compared to their unstrained counterpart. When the film is strained the aggregate order ($1/\sigma$) decreases for both thick and thin films for both incident polarization orientations. In the thin film, absorption of polarized light perpendicular to the strain direction has a distinctively high σ, or lower aggregate order.

Details of the crystalline P3HT stacking character are provided by grazing incidence X-ray diffraction (GIXD) measurements, which were conducted on the unstrained and strain-aligned thick films with image plate data given in **Figure 3**. In the strained films, the diffraction characteristics are given for the X-ray beam oriented parallel and perpendicular to the strain direction. The diffraction pattern of the unstrained film is typical for a P3HT:PCBM BHJ film where the P3HT is observed to have a slight preference for edge on stacking (conjugated ring plane perpendicular to the substrate) with a broad out-of-plane π–π stacking orientation distribution, and a diffuse PCBM ring found near 1.4 Å^{-1}.[20] When the film is strained by 100%, a distinct difference in P3HT diffraction is found under orthogonal X-ray beam directions, while the diffuse scattering from PCBM remains similar. When the X-ray beam is parallel to the strain direction (scattering vector is nominally perpendicular to the strain direction), the P3HT crystals oriented with the polymer

backbone parallel to the strain direction have a similar out of plane stacking distribution as the isotropic film with a slight increase in face-on stacking (conjugated ring plane parallel to the strain direction). When the X-ray beam is perpendicular to the strain direction, a significant drop off in intensity is found for off-normal diffraction. While the intensity in the two directions cannot be quantitatively compared due to differences in scattering volume and exposure time, the lack of diffraction is indicative of a very small amount of P3HT crystals with their backbone aligned perpendicular to the strain direction, consistent with previous work on strain-aligned neat P3HT films.[14,15]

The absorbance and GIXD show evidence that both the highly ordered P3HT aggregates and the crystalline aggregates are primarily oriented in the direction of strain. However, high order aggregates that are not perfectly aligned parallel to the direction of the strain will contribute to absorption of perpendicular-polarized light. To consider the magnitude of this contribution, we consider previous work on aligned P3HT films where GIXD φ-scans were measured on 100% strained films.[14] These films had a dichroic ratio of approximately 4.0 at 605 nm, similar to but lower than the dichroic ratio of the aligned films in this study. The ϕ-scan considered the diffraction intensity of the in-plane 100 peak as the film is rotated azimuthally, which is considered the characteristic orientation distribution for all crystals in the film. While aggregates do not necessarily diffract,[21] the crystal distribution provides an approximation of the high order aggregate in-plane orientation distribution. Based on this assumption, the contribution of the high order aggregate absorption for light polarized perpendicular to the strain direction is estimated to be approximately 2%, with details of the analysis provided in the Supporting Information. Thus, while absorption of light polarized parallel to the strain direction may have contributions from both high and low order aggregates, absorption of light polarized perpendicular to the strain direction is found to be primarily from more disordered P3HT aggregates.

2.2. Internal Quantum Efficiency

To probe how light absorption in the distinct polymer aggregates influences device performance, we determine the internal quantum efficiency (IQE) of the unstrained and strain-aligned OPV cells under linearly polarized illumination. The IQE is the ratio of the number of charges extracted from the device to the number of photons absorbed by the active layer,[22] and is found by dividing the external quantum efficiency (EQE) by the absorption of the active layer. The EQE of all devices under polarized illumination is given in **Figure 4**. A large anisotropy is observed in the EQE that is primarily attributed to the differences in device absorption.

The active layer absorption in the device is measured using a combination of an integrating sphere reflection-based measurement and a transfer matrix model (TMM).[22] The reflection-mode integrating sphere measurement is used to obtain the full absorption of the device stack including electrodes. The TMM is used to predict the absorption of all layers of the OPV cell excluding the active layer, i.e., the parasitic absorption. The

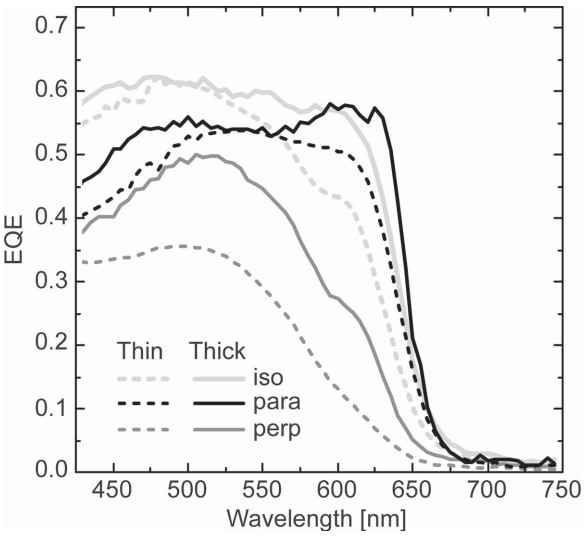

Figure 4. External quantum efficiency (EQE) for the unstrained film (iso) and strain-aligned films under polarized light parallel (para) and perpendicular (perp) to the strain direction.

active layer absorption is then calculated by subtracting the parasitic absorption from the total device stack absorption, given in **Figure 5** for the strain-aligned OPV cells.[22] The active layer absorption for the isotropic devices is given in Figure S2, Supporting Information. It is important to note that anisotropic optical constants for the P3HT:PCBM layer were required to accurately calculate the parasitic absorption with the TMM for the strain-aligned devices. While the P3HT:PCBM layer is not included in the parasitic absorption, the electric field intensity distribution throughout the device stack is affected by the optical constants of this layer and thus should be representative of the film. The anisotropic refractive index was estimated by using previous ellipsometry measurements of strain-aligned P3HT films,[14] and taking the films as a 50:50 ratio by volume of aligned P3HT and isotropic PCBM. The imaginary part of the refractive index was then scaled slightly further to capture the larger dichroic ratio of the aligned BHJ films as compared to the aligned neat P3HT films. The scaling was such that the experimentally determined total reflection of the cell closely matched the modeled reflection, as given in Figure S4, Supporting Information. Finally, a film roughness was also introduced in the TMM to accurately reproduce the measured absorption at wavelengths greater than 650 nm.[23] The input roughness values ranged from 2–7 nm and agree well with the surface roughness of the P3HT:PCBM layer as measured by atomic force microscopy.

From the EQE and active layer absorption, the IQE for each device is determined with results for OPV cells under polarized light provided in **Figure 6**. The IQE for the unstrained devices is found to be similar to previous results for high performing P3HT:PCBM OPV devices,[4,22] without significant separation with incident polarization direction, as expected. In the strain-aligned devices, it is observed that the IQE spectra are also independent of incident light polarization. The IQE of these films is similar to the IQE of the unstrained devices, with a slight drop at shorter wavelengths. The IQE data are limited to

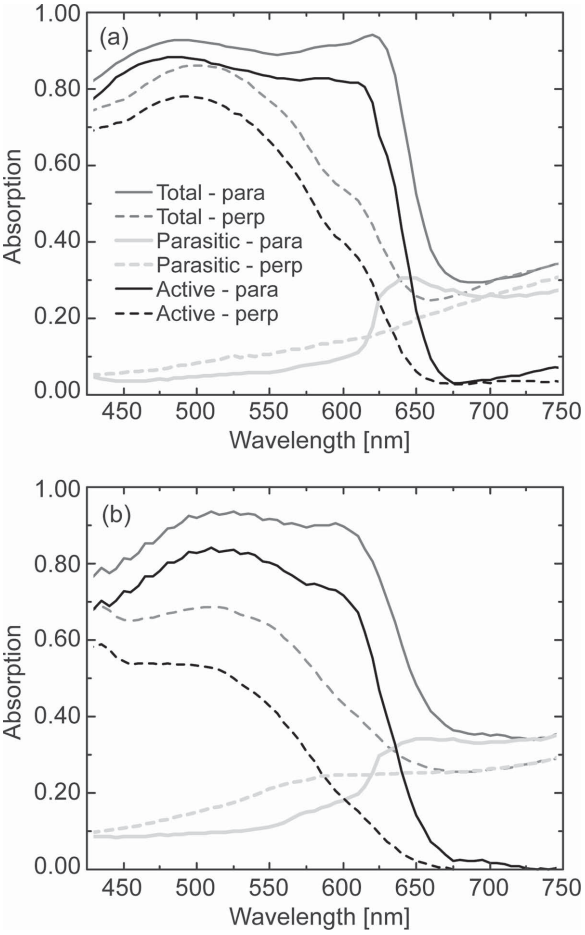

Figure 5. Light absorption in the a) thin and b) thick strain-aligned films. The active layer absorption (active) is determined by subtracting the parasitic absorption calculated using transfer matrix modeling from the experimentally measured total (total) device absorption. The absorption is measured under polarized light parallel (para) and perpendicular (perp) to the strain direction.

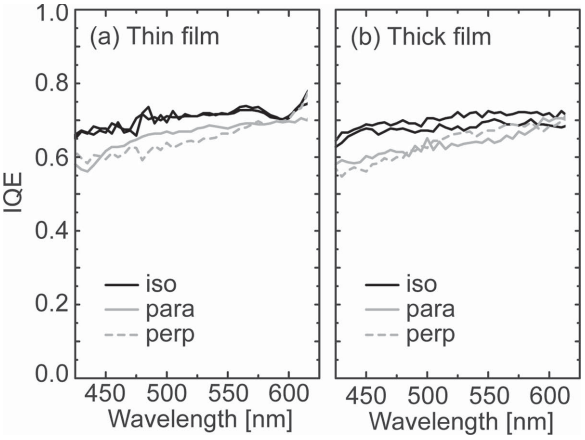

Figure 6. Internal quantum efficiency (IQE) for the unstrained (iso) and strain-aligned BHJ device under polarized light parallel (para) and perpendicular (perp) to the strain direction for the a) thin film and b) thick film devices.

wavelengths below ≈620 nm due to the near-zero light absorption past this wavelength.

2.3. Light Intensity Device Measurements

The H-aggregate model fits to the measured absorbance show that for light absorption of polarized light perpendicular to the strain direction, the P3HT aggregates are highly disordered. This level of disorder in P3HT:PCBM films has previously been shown to result in significant space charge effects,[18] and increased bimolecular recombination rates[7] that limit device performance. Light intensity measurements are a simple and effective tool that can assist in determining the order of recombination (i.e., monomolecular vs bimolecular) as well as space charge effects and are thus investigated with this set of devices.[2,9,24,25]

The light intensity (I) dependence of the short circuit current (J_{SC}) and open circuit voltage (V_{OC}) is given in **Figure 7** for the thin film, and in Figure S5, Supporting Information, for the thick film devices. The J_{SC} dependence on I is found to follow the relationship, $J_{SC} \propto I^m$,[9,17] where scaling factor, m, is found to be close to 1 for all films (unstrained and strain-aligned) and under the two polarized light orientations. As m approaches 1, it has been shown that charge recombination is primarily monomolecular.[9,26] Conversely, if space charge effects are a factor, the scaling factor is typically found to be significantly less than 1.[17] The linear dependence between J_{SC} and I highlights that there is efficient charge transport through the device and space charge effects are not significant. As the P3HT:PCBM device moves away from short circuit current and toward open circuit conditions, there is commonly a transition from monomolecular recombination to contributions from bimolecular and Shockley Read Hall (SRH) processes.[25] When bimolecular recombination is the sole loss mechanism, the slope of V_{OC} with $\ln(I)$ is equivalent to $k_B T/e$, where k_B is Boltzmann constant, T is temperature, e is the electron charge.[25] In P3HT:PCBM BHJ OPV cells, the slope is typically found to be greater than $k_B T/e$, attributed to a contribution from charge recombination of SRH nature. The V_{OC} as a function of illumination is given in Figure 7b for the thin film and Figure S5b, Supporting Information, for the thick film devices. The slope of the data is found to be similar to other reports on high performance P3HT:PCBM OPV cells,[25] and no significant differences are found between the unstrained and strained devices or between the two incident polarized light directions. In summary, the light intensity measurements show that the dominant recombination mechanisms in the device follow similar trends commonly observed for high performance P3HT:PCBM OPV cells, and that no distinct recombination processes are observed between the unstrained and strain-aligned OPV cells.

2.4. Discussion

In OPV cells, the IQE can be broken down into the efficiency of exciton diffusion to the heterojunction, exciton dissociation into free charge carriers, and charge collection. When considering various loss mechanisms, previous work has suggested that

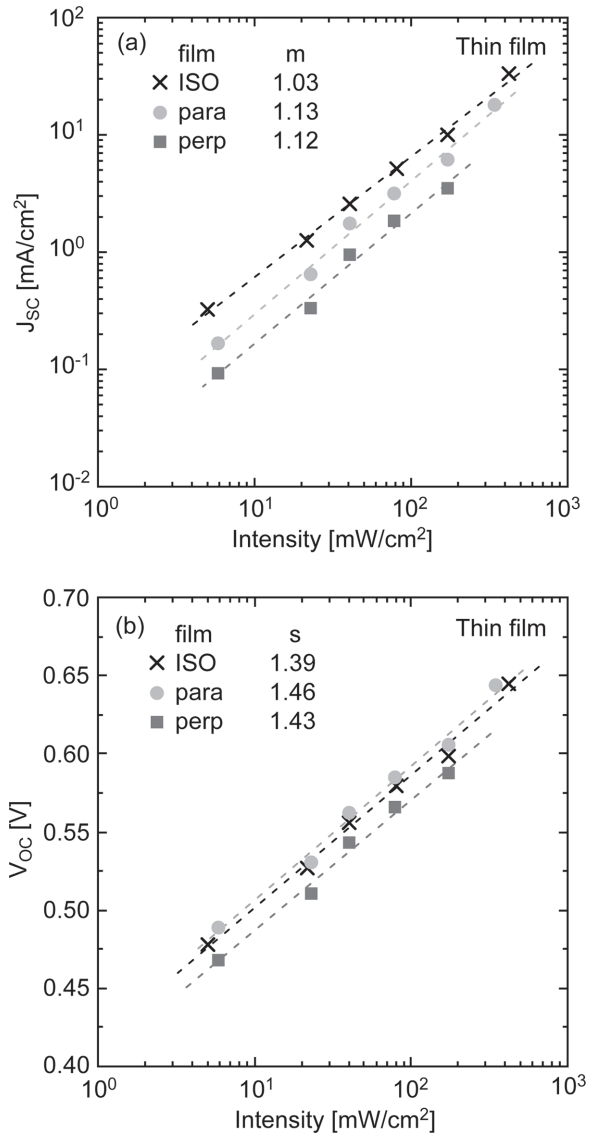

Figure 7. a) Short circuit current (J_{SC}) with varying light intensity for the unstrained (iso) and strain aligned films under parallel (para) and perpendicular (perp) polarized light for the thin films. The line fits are given with the slope *m* provided in the legend. b) The open circuit voltage (V_{OC}) with varying light intensity for the unstrained and strain-aligned films. The data are given with a natural log curve fit with a slope of sk_BT/e, with s provided in the legend. The illumination is for simulated solar AM1.5G light.

geminate recombination at the heterojunction is a significant loss mechanism in disordered P3HT:PCBM devices.[3,11] However, more recently, bias-enhanced charge extraction (BACE) measurements have provided evidence that geminate recombination is not a significant loss mechanism in these cells over a wide range of morphological order.[7] This suggests that the predominate loss mechanism in disordered P3HT:PCBM solar cells originates from poor charge collection efficiency. In P3HT:PCBM BHJ films, efficient and extremely fast exciton quenching is typically observed.[3,27] This suggests that in the films under consideration, electronic coupling to the heterojunction is efficient and the exciton does not travel between P3HT domains. Thus, the similar IQE for light absorbed by the ordered and disordered P3HT aggregates in the aligned films provides direct evidence that exciton dissociation into free charge carriers is efficient in films of various P3HT local order (i.e., the quantum efficiency of photogeneration of charge carriers is independent of P3HT aggregate order) supporting recent findings.[7]

Assuming that the photogenerated exciton dissociates into free carriers at the nearest heterojunction interface, the hole is either introduced into the high or low order P3HT aggregates associated with the location of light absorption. The similar polarization-dependent IQE in the aligned BHJ devices also shows that photogenerated charge collection is independent of the local order at the heterojunction. Previous work has shown that space charge limited photocurrent becomes an important factor in BHJ films when W is greater than ≈150 meV and σ is greater than ≈77 meV.[18] While the absorption of perpendicular polarized light in the strain-aligned films is found to have fitting parameters with greater W and σ, space charge effects are not observed in the films. This suggests that the hole introduced into the disordered P3HT effectively moves to an ordered polymer network for efficient charge collection. In the strained films, the majority of P3HT aggregates are aligned in the direction of strain, and are similar in order to high performance BHJ films.[18] Therefore, once the hole moves away from the heterojunction it will see a similar P3HT environment of a high performance BHJ films, and efficient carrier sweep out is possible. This picture is consistent with the BHJ description that P3HT and PCBM segregation results in ordered regions that have a favorable shift in the local molecular energy levels compared to the disordered regions providing a driving force for charge dissociation and a path for efficient carrier collection.[6,10,11]

Finally, the IQE in the strained films is found to have a slight decrease in IQE as compared to their unstrained counterparts, particularly for shorter wavelengths. The increasing difference found at shorter wavelengths corresponds to an increasing contribution of the PCBM absorption to the IQE. Thus, the drop in the strained films may be associated with more isolated PCBM molecules or clusters that do not allow for an efficient electron percolation network. Previous work on polymer:fullerene devices has suggested that isolated PCBM molecules will act as morphological traps and a drop in quantum efficiency will occur across the entire response spectrum of the device.[8] In addition, analysis of P3HT:PCBM OPV cells doped with the fullerene derivative, $PC_{84}BM$, to act as an electron trap, had a similar drop in quantum efficiency across the entire response spectrum of the device.[28] The slope of the V_{OC} as a function of illumination intensity in this study was also found to be sensitive to fullerene trap density.[28] Here, we do observe a small drop in IQE across the spectrum, suggesting that a small contribution from PCBM trap states may be possible. However, illumination intensity dependent device behavior does not significantly vary in the strained devices, suggesting this is only a minor factor in device performance (similar to the minor drop in IQE). The fact that the films are physically strained by 100% while maintaining IQEs associated with high performance P3HT:PCBM BHJ devices speaks to effectiveness of this alignment approach.

3. Conclusion

In this study we demonstrated an experimental procedure that allows us to study performance losses associated with light absorption by high and low order polymer aggregates in a single BHJ solar cell. In order to do so we applied a 100% uniaxial strain on ductile P3HT:PCBM BHJ films. This results in a film with a high degree of polymer alignment, particularly of the crystalline P3HT. The devices are then tested under linearly polarized light, where polarized light parallel to the strain direction is found to be absorbed predominately by amorphous P3HT and high order P3HT aggregates, and light polarized perpendicular to the strain direction is absorbed by amorphous and lower order polymer aggregates. The IQE for the strain-aligned devices was found to be similar under each polarization, indicating that the efficiency of charge photogeneration is efficient for excitons generated in both high and low order P3HT aggregates. Once excitons dissociated into free charge, the BHJ morphology is such that sweep out of charge carriers is efficient. This is supported by varying-light intensity measurements that show no presence of bimolecular recombination under short circuit conditions. This device architecture overcomes space charge effects that have previously dominated IQE losses that have made it difficult to probe the losses at the heterojunction interface associated with film disorder. Thus, the demonstrated method of orienting distinct morphological features in the plane of the film has the unique and significant capacity to determine if recombination losses associated with polymer morphology occur in the film bulk or near the heterojunction interface. Since the low and high order aggregates are probed within the *same* film, we were able to normalize any differences in charge collection efficiency that are typically present between low and high order BHJ films. The approach of fabricating in-plane aligned polymer BHJ OPV devices is expected to be possible in a number of polymer systems,[29] and as shown in this study, is a simple and highly effective tool to gain insight into device performance.

4. Experimental Section

Materials: The P3HT was obtained from Plextronics Inc. with a number-averaged molecular mass M_n = 50 kD, a regioregularity of 99%, and a polydispersity of 2.1.[30] The PCBM was obtained from Nano-C with a purity of 99.5%. The PEDOT:PSS solution was type PVP AI4083, obtained from Heraeus Materials Technology.

Device Preparation: The device fabrication starts with spin casting PEDOT:PSS films at 5000 rpm onto a donor glass substrate followed by thermal annealing at 120 °C for 20 min. Two P3HT:PCBM solutions were used, with a 60:40 mass ratio in 1,2-dichlorobenzene at a concentration of 20 mg mL^{-1} and 36 mg mL^{-1}. The P3HT:PCBM film was then spun cast at 1000 rpm for 60 s, resulting in a ≈85 nm and a ≈220 nm thick film, respectively, as determined by variable angle spectroscopic ellipsometry. The P3HT:PCBM film on the PEDOT:PSS coated glass substrate was then laminated onto a PDMS slab that was attached to a custom built strain stage. The composite stack was immersed in a deionized (DI) water bath where the PEDOT:PSS layer dissolves and the donor substrate detaches from the film. The P3HT:PCBM film, which is now adhered to the PDMS slab, was removed from the DI water and dried with N_2 gas. The composite was then strained to 100% (*strained film*) or left unstrained and printed onto a receiving substrate that consists of spun cast PEDOT:PSS film on an indium tin oxide (ITO) coated glass substrate. The PDMS was then removed, leaving the P3HT:PCBM film on the receiving substrate. In order for the strain alignment method to be successful, the P3HT:PCBM film must be highly deformable, which has previously been shown to depend on the local order of the P3HT in the blend film.[31] The designated solution formulation and casting conditions, described above, resulted in a relatively low level of local order. This resulted in the ability to strain the films, by over 100%, without fracturing or tearing. After the strain and print process, the local order of the P3HT:PCBM is improved and OPV device performance is optimized by thermally annealing the films at 130 °C for 10 min, followed by slowly cooling the films to room temperature. To complete the OPV cell, the cathode, consisting of 1 nm of LiF and 100 nm Al, was deposited by vacuum thermal evaporation at a pressure of 1×10^{-6} mbar.

Morphology Characterization: Absorbance measurements were made using an Ocean Optics Jazz spectrometer. X-ray diffraction was performed at the Stanford Synchrotron Radiation Lightsource (SSRL) on beam line 11–3 with an area detector (MAR345 image plate), an energy of 12.735 keV, and an incidence angle of ≈0.12°.

Device Characterization: The active area of the OPV cell was 3.14 mm^2 and the devices were tested using a Newport 150 W solar simulator with an AM1.5G filter under linear polarized light at an intensity of 41 mW cm^{-2}. The EQE measurement was performed using a Newport 7400 Cornerstone 130 1/8m monochromator and a Stanford Research Systems SR810 Lock-in amplifier.

Supporting Information

Supporting information is available from the Wiley Online Library of from the author.

Acknowledgements

This research work was supported by the National Science Foundation (Award No. 1200340). Portions of this research were carried out at the Stanford Synchrotron Radiation Lightsource, a Directorate of SLAC National Accelerator Laboratory, and an Office of Science User Facility operated for the U.S. Department of Energy Office of Science by Stanford University. The authors thank Michael F. Toney for assistance with the X-ray diffractions measurements.

Received: September 26, 2014
Revised: December 5, 2014
Published online: January 21, 2015

[1] G. Yu, J. Gao, J. C. Hummelen, F. Wudl, A. J. Heeger, *Science* **1995**, *270*, 1789.
[2] C. M. Proctor, M. Kuik, T. Q. Nguyen, *Prog. Polym. Sci.* **2013**, *38*, 1941.
[3] I. A. Howard, R. Mauer, M. Meister, F. Laquai, *J. Am. Chem. Soc.* **2010**, *132*, 14866.
[4] G. F. Burkhard, E. T. Hoke, S. R. Scully, M. D. McGehee, *Nano Lett.* **2009**, *9*, 4037.
[5] a)J. R. Tumbleston, D. H. Ko, E. T. Samulski, R. Lopez, *Phys. Rev. B* **2010**, *82*, 205325; b)C. Deibel, T. Strobel, V. Dyakonov, *Phys. Rev. Lett.* **2009**, *103*, 036402.
[6] F. C. Jamieson, E. B. Domingo, T. McCarthy-Ward, M. Heeney, N. Stingelin, J. R. Durrant, *Chem. Sci.* **2012**, *3*, 485.
[7] J. Kniepert, I. Lange, N. J. van der Kaap, L. J. A. Koster, D. Neher, *Adv. Energy Mater.* **2014**, *4*, 1301401.
[8] J. A. Bartelt, Z. M. Beiley, E. T. Hoke, W. R. Mateker, J. D. Douglas, B. A. Collins, J. R. Tumbleston, K. R. Graham, A. Amassian, H. Ade,

J. M. J. Frechet, M. F. Toney, M. D. McGehee, *Adv. Energy Mater.* **2013**, *3*, 364.
[9] S. R. Cowan, A. Roy, A. J. Heeger, *Phys. Rev. B* **2010**, *82*, 245207.
[10] Y. Kim, S. Cook, S. M. Tuladhar, S. A. Choulis, J. Nelson, J. R. Durrant, D. D. C. Bradley, M. Giles, I. Mcculloch, C. S. Ha, M. Ree, *Nat. Mater.* **2006**, *5*, 197.
[11] T. M. Clarke, A. M. Ballantyne, J. Nelson, D. D. C. Bradley, J. R. Durrant, *Adv. Funct. Mater.* **2008**, *18*, 4029.
[12] G. Li, V. Shrotriya, J. S. Huang, Y. Yao, T. Moriarty, K. Emery, Y. Yang, *Nat. Mater.* **2005**, *4*, 864.
[13] O. Awartani, M. W. Kudenov, B. T. O'Connor, *Appl. Phys. Lett.* **2014**, *104*, 093306.
[14] B. O'Connor, R. J. Kline, B. R. Conrad, L. J. Richter, D. Gundlach, M. F. Toney, D. M. DeLongchamp, *Adv. Funct. Mater.* **2011**, *21*, 3697.
[15] B. T. O'Connor, O. G. Reid, X. Zhang, R. J. Kline, L. J. Richter, D. J. Gundlach, D. M. DeLongchamp, M. F. Toney, N. Kopidakis, G. Rumbles, *Adv. Funct. Mater.* **2014**, *24*, 3422.
[16] M. C. Gurau, D. M. Delongchamp, B. M. Vogel, E. K. Lin, D. A. Fischer, S. Sambasivan, L. J. Richter, *Langmuir* **2007**, *23*, 834.
[17] V. D. Mihailetchi, J. Wildeman, P. W. M. Blom, *Phys. Rev. Lett.* **2005**, *94*, 126602.
[18] S. T. Turner, P. Pingel, R. Steyrleuthner, E. J. W. Crossland, S. Ludwigs, D. Neher, *Adv. Funct. Mater.* **2011**, *21*, 4640.
[19] a) F. C. Spano, *J. Chem. Phys.* **2005**, *122*, 234701; b) F. C. Spano, *Chem. Phys.* **2006**, *325*, 22.
[20] E. D. Gomez, K. P. Barteau, H. Wang, M. F. Toney, Y. L. Loo, *Chem. Commun.* **2011**, *47*, 436.
[21] D. T. Duong, M. F. Toney, A. Salleo, *Phys. Rev. B* **2012**, *86*, 205205.
[22] G. F. Burkhard, E. T. Hoke, M. D. McGehee, *Adv. Mater.* **2010**, *22*, 3293.
[23] a) K. H. An, B. O'Connor, K. P. Pipe, M. Shtein, *Org. Electron.* **2009**, *10*, 1152; b) C. C. Katsidis, D. I. Siapkas, *Appl. Opt.* **2002**, *41*, 3978.
[24] V. D. Mihailetchi, H. X. Xie, B. de Boer, L. J. A. Koster, P. W. M. Blom, *Adv. Funct. Mater.* **2006**, *16*, 699.
[25] G. J. A. H. Wetzelaer, M. Kuik, P. W. M. Blom, *Adv. Energy Mater.* **2012**, *2*, 1232.
[26] J. R. Tumbleston, Y. C. Liu, E. T. Samulski, R. Lopez, *Adv. Energy Mater.* **2012**, *2*, 477.
[27] J. Kniepert, M. Schubert, J. C. Blakesley, D. Neher, *J. Phys. Chem. Lett.* **2011**, *2*, 700.
[28] S. R. Cowan, W. L. Leong, N. Banerji, G. Dennler, A. J. Heeger, *Adv. Funct. Mater.* **2011**, *21*, 3083.
[29] a) D. M. DeLongchamp, R. J. Kline, Y. Jung, D. S. Germack, E. K. Lin, A. J. Moad, L. J. Richter, M. F. Toney, M. Heeney, I. McCulloch, *ACS Nano* **2009**, *3*, 780; b) H. R. Tseng, L. Ying, B. B. Y. Hsu, L. A. Perez, C. J. Takacs, G. C. Bazan, A. J. Heeger, *Nano Lett.* **2012**, *12*, 6353.
[30] Certain commercial equipment, or materials are identified in this paper in order to specify the experimental procedure adequately. Such identification is not intended to imply recommendation or endorsement by the National Institute of Standards and Technology, nor is it intended to imply that the materials or equipment identified are necessarily the best available for the purpose.
[31] O. Awartani, B. I. Lemanski, H. W. Ro, L. J. Richter, D. M. DeLongchamp, B. T. O'Connor, *Adv. Energy Mater.* **2013**, *3*, 399.